

Subpicosecond pulse laser absorption by an overdense plasma with variable ionization

Alexei Zhidkov and Akira Sasaki

Advanced Photon Research Center, Japan Atomic Energy Research Institute, 25-1, Mii-minami-cho, Neyagawa-shi, Osaka 572, Japan

(Received 6 July 1998; revised manuscript received 26 January 1999)

Transient ionization of an overdense plasma produced by a subpicosecond, p -polarized obliquely incident pulse laser of moderate intensity (10^{16} – 10^{18} W/cm²) changes the plasma heat transfer via processes dominated by the return current and the absorption rate via ion acceleration. To explore the effect of variable ionization, a hybrid one-dimensional electro-magnetic particle-in-cell method that conforms to a direct solution of the Fokker-Planck-Landau equation is applied. A method that includes the Langevin equation to account for Coulomb collisions and the average ion model to calculate the nonlocal thermodynamic equilibrium ionization balance provides good agreement between the computed absorption and the measured results.
[S1063-651X(99)03906-9]

PACS number(s): 52.40.Nk, 52.25.Jm, 52.65.Rr

I. INTRODUCTION

An overdense plasma irradiated by a subpicosecond pulse laser of moderate intensity ($I = 10^{16}$ – 10^{18} W/cm²) is considered as an efficient, high brightness, tabletop 1–10 keV x-ray source [1–5]. Although the x-ray emission should be well characterized for optimization in any application, the present experimental diagnostics have limited temporal and spectral resolution. Therefore, the self-consistent simulation of the laser absorption and heat flow combined with atomic kinetics inside the plasma, which can predict the time-dependent x-ray intensity and spectrum, is extremely desirable.

The complexity of the subpicosecond pulse laser interaction with a solid-density plasma has been shown in a number of papers [6–17]. The energy of an ultrashort pulse laser is absorbed by the plasma with a steep density gradient through collisional and collisionless processes including the resonance absorption, anomalous skin effect, and vacuum heating. When an intense laser pulse irradiates the target, high energy electrons can be produced from a variety of interactions such as direct acceleration by the laser electric field or by the resonant excitation of plasma waves. In high density plasmas collisions may dominate the temporal and spatial evolution of the energy distribution of electrons, and their relaxation and transport, eventually resulting in thermalization of electrons and heating of the plasma. In this case, absorption of the laser also strongly depends on the atomic kinetics inside the plasma. In the case of ultrashort pulse laser irradiation, the time required to ionize significantly the target material is comparable to the pulse duration. Subsequent increases of electron density and ion charges during the laser pulse modify the rate of absorption and the penetration depth of the heat front into the target.

The strong effect of variable ionization on heat transfer in a solid-density carbon plasma has been shown in [15]; the collisional absorption has been used assuming a normal incidence laser and the laser absorption has not been calculated self-consistently. When an obliquely incident p -polarized pulse laser irradiates the target, the principal process responsible for the high absorption efficiency is the resonance absorption. The absorption efficiency is changed by the ion acceleration [12], and the heat flow is dominated by the re-

turn current [16], which strongly depends on the plasma conductivity. The transient plasma ionization obviously plays a key role in both cases. Moreover, a recent experiment [17] has displayed the strong dependence of the plasma reflectivity on the prepulse delay. In the experiment the plasma reflectivity for the same ($T = 120$ fs, $\lambda = 800$ nm, 45° p -polarized) laser pulse changed from 35% to more than 90% with the prepulse delay increased from 4 to 18 ps. A detailed analysis of the variable ionization effect is crucial to find ways to increase the x-ray brightness and/or to reproduce the spectroscopy measurements.

For moderate laser intensities, an x-ray source simulation is supposed to start from an initially cold solid-density plasma that is rapidly heated to some hundred eV. To foresee the plasma x-ray emission we have to know the absorption, heat flow, and ionization dynamics in plasmas. But these processes cannot be described in the framework of classical Fresnel and Spitzer-Harm theories and local thermodynamic equilibrium (LTE) ionization balance during laser-plasma interaction [13,15]. In the present work, we carry out self-consistent modeling of the absorption of a p -polarized short-pulse laser by such a plasma which is the basic component of an x-ray emission simulation. Our main goal is to understand the effect of elastic and inelastic collisions on the absorption efficiency and heat transfer when the collisionless absorption is not negligible. To overcome the problem of self-consistent solution of the Fokker-Planck-Landau (FPL) equation for plasma electrons along with ionization dynamics and the Maxwellian curl equations for laser fields we suggest one-dimensional in the conventional space and three-dimensional in the velocity space (1D3V) electromagnetic particle-in-cell (PIC) simulation [18] with the Langevin equation that conforms to a direct solution of the FP equation [19]. The laser prepulse [17] is supposed to produce an initial plasma density distribution and to preheat the plasma.

To include atomic physics processes a new method is developed by adding a ‘kinetics’ grid for macroscopic parameters of plasma such as the density, temperature, average charge, and level population, and by allowing a superparticle (particles used in numerical simulation) charge to be changed according to the average ion model. To provide the statistics, a ‘kinetics’ cell includes many PIC cells.

The paper consists of three parts. In the first part the method employed is described. In the second part the heat flow and ionization balance in a carbon plasma irradiated by an s -polarized pulse are presented. A good agreement of the results with those of the direct solution of the FPL equation ([15]) is shown. In the third part, the absorption efficiency of a p -polarized pulse laser and the heat flow in a Si plasma with variable ionization, taking into account the effect of laser prepulse, are discussed. The strong effect of elastic collisions and variable ionization on the heat transfer is demonstrated. The role of the return current in energy deposition and ionization dynamics is revealed.

II. GENERAL EQUATIONS

Nonideality and degeneracy of plasma electrons are the main problems in the simulation of solid-density plasma and laser interactions at moderate laser intensities. These problems arise because the plasma is initially cold. The parameter of ideality,

$$\Gamma_{ei} = e^2(4\pi N_e/3)^{1/3}/T_e,$$

is equal to unity at $T_e = \varepsilon_F$, where the Fermi energy is already about 5–10 eV. At lower temperatures, plasma electrons degenerate and cannot be considered as particles. To avoid such problems we have to assume that a plasma is heated by a laser prepulse to a temperature when $\Gamma_{ei} < 1$ and electrons can be treated as particles, but the temperature is still small enough (10–20 eV, see [13,15]) to simulate the plasma ionization dynamics and the transient x-ray emission.

The self-consistent simulation of a nondegenerate, solid-density plasma should be based on the FPL equation with the collisional integral in the Balescu-Lennard form [20,21],

$$\left[\frac{\partial f_a}{\partial t} \right]_{\text{col}} = \frac{\partial}{\partial p_{ai}} \sum_b \int d\mathbf{p}_b w_{ij}^{ab}(\mathbf{v}_a, \mathbf{v}_b) \left(\frac{\partial f_a}{\partial p_{aj}} f_b - \frac{\partial f_b}{\partial p_{bj}} f_a \right), \quad (1)$$

$$w_{ij}^{ab} = \pi \int \frac{d\mathbf{k}}{(2\pi)^3} \left(\frac{4\pi e_a e_b}{k^2} \right)^2 \frac{k_i k_j \delta(\mathbf{k} \cdot \mathbf{v}_a - \mathbf{k} \cdot \mathbf{v}_b)}{|\varepsilon(\mathbf{k}, \mathbf{v}_a, \mathbf{k})|^2},$$

where $f_a(\mathbf{p}_a)$ is the distribution function of particles a and $\varepsilon(\mathbf{k}, \mathbf{v}, \mathbf{k})$ is the plasma permittivity. For $\varepsilon = 1$ Eq. (1) is the well-known Landau collisional integral. To avoid the complexity of calculation in Eq. (1) we also assume that the effect of permittivity is only in the value of Coulomb logarithm Λ , in the FPL equation [22]—the effective collision approximation. Hence the Coulomb logarithm Λ is the parameter of plasma collisionality. Then following the TKN approximation [23] we set $\Lambda_{\min} = 2$ for an overdense plasma. We should also note that the method presented below allows, in principle, a numerical solution of Eq. (1), but such a solution is difficult.

A. Langevin equation

In the frame of an effective collision approximation for the PIC plasma simulation, that conforms to the modeling based on the FPL equation, we must use the Langevin equation for the motion of charged particles. The equation has the form

$$\frac{d\mathbf{p}_k}{dt} = q_k \left[\mathbf{E}(\mathbf{r}_k) + \frac{\mathbf{p}_k}{\gamma_k c} \times \mathbf{H}(\mathbf{r}_k) \right] + \mathbf{P}_k(\mathbf{v}_k), \quad (2a)$$

where \mathbf{p}_k is the momentum, \mathbf{r}_k is the position, q_k , M_k are charge and mass of a particle, $q_e = -e$, $q_i = Z_k e$, Z_k is the ion charge, and \mathbf{E} and \mathbf{H} are the electric and magnetic fields.

$$\gamma_k = \sqrt{M_k^2 c^4 + c^2 p_k^2}.$$

Here $\mathbf{P}_k(\mathbf{v}_k)$ is the collisional term of the equation including elastic collisions [18] such that

$$\mathbf{P}_k(\mathbf{v}_k) = \mathbf{f}_k + (d_k \xi + g_k \eta). \quad (2b)$$

The term in the brackets is the fluctuating acceleration. ξ , η describe the normal random processes with the same characteristics,

$$\langle \xi_i(t) \rangle = 0, \quad \langle \xi_i(t) \xi_k(t + \Delta t) \rangle = \delta_{ik} \delta(\Delta t), \quad (2c)$$

$$\langle \xi_i(t) \eta_k(t + \Delta t) \rangle = 0, \quad \int_t^{t+\Delta t} \xi_k dt' = p_k \sqrt{\Delta t},$$

where p_k is the normally distributed random number.

To determine functions \mathbf{f}, d, g in Eq. (2b), Eq. (2a) should be integrated in time $[t, t + \Delta t]$ with $\mathbf{E} = \mathbf{H} = 0$. Then by using the solutions of Eq. (2a), the velocity correlation functions $\langle \Delta v_i \rangle$ and $\langle \Delta v_i \Delta v_j \rangle$ can be calculated. In the problem under consideration only non-relativistic particle collisions are important. So the representation of the collisional term is given in the nonrelativistic form, although the equation can be easily transformed to a relativistic form by using Budker's collisional integral. In the limit $\Delta t \rightarrow 0$ the nonrelativistic correlation functions must give the Fokker-Planck coefficients, that are expressed through well-known Rosenbluth potentials [22] for a plasma with a Maxwellian velocity distribution,

$$A_{i\alpha\beta}(\mathbf{v}) = \lim_{\Delta t \rightarrow 0} \frac{1}{\Delta t} \langle \Delta v_{i\alpha\beta} \rangle = N_\beta \int f_\beta(\mathbf{v}_\beta) w_i^{\alpha\beta} d\mathbf{v}_\beta, \quad (2d)$$

$$B_{ik\alpha\beta}(\mathbf{v}) = \lim_{\Delta t \rightarrow 0} \frac{1}{\Delta t} \langle \Delta v_{i\alpha\beta} \Delta v_{j\alpha\beta} \rangle = N_\beta \int f_\beta(\mathbf{v}_\beta) w_{ij}^{\alpha\beta} d\mathbf{v}_\beta,$$

where

$$w_i^{\alpha\beta} = - \left(\frac{\mu_{\alpha\beta}}{M_\alpha} \right) (v_{i\alpha} - v_{i\beta}) |\mathbf{v}_\alpha - \mathbf{v}_\beta| \sigma_1(|\mathbf{v}_\alpha - \mathbf{v}_\beta|), \quad (2e)$$

$$w_{ij}^{\alpha\beta} = \left(\frac{\mu_{\alpha\beta}}{M_\alpha} \right)^2 |\mathbf{v}_\alpha - \mathbf{v}_\beta|^3$$

$$\times \left[\delta_{ij} \frac{\sigma_2}{2} + \frac{(v_{i\alpha} - v_{i\beta})(v_{j\alpha} - v_{j\beta})}{|\mathbf{v}_\alpha - \mathbf{v}_\beta|^2} \left(2\sigma_1 - \frac{3}{2}\sigma_2 \right) \right]$$

are the velocity correlation functions inherent to elastic collisions with the transport cross sections

$$\sigma_1 = \int (1 - \cos \theta) d\sigma, \quad \sigma_2 = \int (1 - \cos^2 \theta) d\sigma.$$

The differential cross section $d\sigma$ depends on a collisional process. The reduced mass μ_{ab} is determined in the conventional way.

The normalized matrices \mathbf{f}, d, g can be present in the following form [18]:

$$f_i = A_i - \aleph(d_{jk} + g_{jk}) \frac{\partial(d_{ik} + g_{ik})}{\partial v_j}, \quad (2f)$$

$$d_{ik} = \frac{1}{\sqrt{2}} (B_{+}^{1/2})_{ik}, \quad g_{ik} = \frac{1}{\sqrt{2}} (B_{-}^{1/2})_{ik},$$

where $B_{(-)}^{1/2}$ and $B_{(+)}^{1/2}$ are the roots of the matrix B . The parameter \aleph in Eq. (2f) equals zero for collision of same-mass particles and equals $\frac{1}{2}$ for collision of light particles with infinite-mass particles. By substituting the Coulomb cross sections

$$\sigma_1(|\mathbf{v} - \mathbf{v}'|) = \frac{1}{2} \sigma_2(|\mathbf{v} - \mathbf{v}'|) = \frac{4\pi e^2 \alpha^2 e^2 \Lambda}{\mu_{\alpha\beta}^2 |\mathbf{v} - \mathbf{v}'|^4}$$

into Eq. (2d) and by assuming further that the distribution function of scatterers in the $e-e$ collision term has the eighth momentum Grad approximation form

$$f(\mathbf{v}) = \frac{N}{\pi^{3/2} v_T^3} \exp\left(-\frac{(\mathbf{v} - \mathbf{u})^2}{v_T^2}\right) \times \left[1 - \frac{\mathbf{q}(\mathbf{v} - \mathbf{u})}{v_T^4} \left(1 - \frac{2}{5} \frac{(\mathbf{v} - \mathbf{u})^2}{v_T^2}\right)\right], \quad (3a)$$

where the thermal velocity v_T and the heat flow \mathbf{q} are

$$v_T^2 = \frac{2}{3} \langle (\mathbf{v} - \mathbf{u})^2 \rangle, \quad \mathbf{q} = \langle (\mathbf{v} - \mathbf{u})^2 (\mathbf{v} - \mathbf{u}) \rangle,$$

with \mathbf{u} the mean velocity, and for electron-electron and electron-ion collisional terms we get the equation [18]

$$\mathbf{P}_e = -4\pi\Lambda \left(\frac{Ze^2}{m_e}\right)^2 \times \left(\frac{m_e}{M_i} N_i \frac{\mathbf{v}}{v^3} + \frac{4}{v_T^2} N_e \frac{\mathbf{w}}{w} G(w) - N_e \Phi'(w) \frac{4(\mathbf{q} \cdot \mathbf{w})}{5v_{T_e}^4} \mathbf{w}\right) + \frac{e^2}{m_e} \left(\frac{4\pi\Lambda Z^2 N_i}{v}\right)^{1/2} \left(\xi - \frac{\mathbf{v}(\mathbf{v}\xi)}{v^2}\right) + \frac{e^2}{m_e} \left(\frac{4\pi\Lambda N_e}{v_{T_e} w}\right)^{1/2} \left[\sqrt{\Phi(w) - G(w)} \left(\zeta - \frac{\mathbf{w}}{w^2}(\mathbf{w}, \zeta)\right) + \sqrt{2G(w)} \frac{\mathbf{w}}{w^2}(\mathbf{w}, \eta)\right]. \quad (3b)$$

In Eq. (3) $\mathbf{w} = (\mathbf{v} - \mathbf{u})/v_T$, η, ξ, ζ describe the normal random processes, each of the vectors has three independent components with the mean equal to zero, and the dispersion equals $(2)^{-1/2}$.

$$\Phi(w) = 2 \int_0^w dx e^{-x^2} / \sqrt{\pi},$$

$$G(w) = [\Phi(w) - w\Phi'(w)] / (2w^2).$$

The plasma parameters are determined on the ‘‘kinetics’’ grid. The process ξ describes plasma electron scattering by ions, ζ describes the moment rotation as a result of electron-electron collision, η describes energy redistribution between electrons after collision, providing the system ergodicity even if there is no electromagnetic field in the plasma. Equation (3) conserves the energy of the system of N electrons in contrast to the Monte Carlo methods that conserve energy of two particles. We should note also that a modification of Eq. (3) for electron-ion collisions by including the lowest limit of drift velocity like the Fermi velocity v_F provides the TKN approximation [23] down to a few eV for solid-density plasma of Al.

By using the fifth momentum Grad approximation for the ion distribution function [Eq. (3a) with $\mathbf{q} = \mathbf{0}$] the ion collisional term can be obtained in the following form when electron temperature T_e exceeds the ion temperature T_i :

$$\mathbf{P}_i = -4\pi\Lambda' \left(\frac{(Ze)^2}{M_i}\right)^2 N_i \frac{4}{v_{T_i}^2} \frac{\mathbf{y}}{y} G(y) + \frac{Ze^2}{M_i} \zeta_3 \left(\frac{4\pi\Lambda N_e}{v_{T_e}} \frac{8}{3\sqrt{\pi}}\right)^{1/2} + \frac{(Ze)^2}{M_i} \left(\frac{4\pi\Lambda' N_i}{v_{T_i} y}\right)^{1/2} \left[\sqrt{\Phi(y) - G(y)} \left(\zeta_1 - \frac{\mathbf{y}}{y^2}(\mathbf{y}, \zeta_1)\right) + \sqrt{2G(y)} \frac{\mathbf{y}}{y^2}(\mathbf{y}, \zeta_2)\right],$$

$$\mathbf{y} = (\mathbf{v}_i - \mathbf{u}_i) / v_{T_i}. \quad (3c)$$

ζ_1, ζ_2 describe the random processes for $i-i$ collisions, and ζ_3 describes ones for $i-e$ collisions with energy exchange. \mathbf{u}_i is the ion mean (fluid) velocity, Z is the average ion charge. All macroscopic values are determined in the ‘‘kinetics’’ cell. The Coulomb logarithms Λ, Λ' for $i-i$ and $e-e$ collisions, respectively, may be different.

The dimensionless units used even for an obliquely incident wave have the following form [7–15]: velocity is in c , energy is in $m_e c^2$, electromagnetic fields in $e/(m_e c \omega)$, time in ω^{-1} , the coordinate is in c/ω . In such units the charge density and current are measured in $(\omega_{pl}/\omega)^2$. Here ω and ω_{pl} are the laser and plasma frequencies.

B. Two-wave approximation

Since a two-dimensional simulation needed to take into account all possible absorption processes is still impractical to reproduce the x-ray emission of multiple charged ions in a plasma irradiated by a $T=0.1-10$ ps pulse laser, we try to simplify calculations by reducing the problem to one dimen-

sion. For that we suggest a two-wave approximation (TWA), in the following [9]. In this way we expect to treat correctly the collision absorption, vacuum heating, anomalous skin effect, and resonance absorption.

According to the TWA there are two plane waves in the plasma. The first wave is the incoming laser field propagating inward in the plasma in the X - Y plane at an arbitrary angle θ with respect to the y axis, and the second one represents the reflected portion of the laser field propagating outward through the plasma at the angle θ to its surface. Both waves are coupled by the plasma current. The wave fronts,

$$\varphi_{\pm} = t \pm \sin \theta x + \cos \theta y = \varphi_{\pm}(x, \tau = t + \cos \theta y), \quad (4)$$

of both waves are parallel to the plasma surface. The TWA assumes that there is no distortion of such a wave front during laser-plasma interaction, no backward scattering, and implicitly uses the assumption that $\omega T \gg 1$, where ω is the laser frequency and T is the laser pulse duration. The last assumption is valid even for subpicosecond pulse lasers.

The TWA equations are derived from the two-dimensional Maxwellian curl equations written in the following form:

$$\begin{aligned} \frac{\partial H_z}{\partial y} &= \frac{\partial E_{L,X}}{\partial t} + \left(j_X + \frac{\partial E_{ST,X}}{\partial t} \right), & -\frac{\partial H_z}{\partial x} &= \frac{\partial E_{L,Y}}{\partial t} + \left(j_Y + \frac{\partial E_{ST,Y}}{\partial t} \right), \\ \frac{\partial E_{L,Y}}{\partial x} - \frac{\partial E_{L,X}}{\partial y} &= -\frac{\partial H_z}{\partial t}, & \frac{\partial E_{ST,X}}{\partial x} + \frac{\partial E_{ST,Y}}{\partial y} &= \rho, & \frac{\partial j_X}{\partial x} + \frac{\partial j_Y}{\partial y} &= -\frac{\partial \rho}{\partial t}, \end{aligned} \quad (5)$$

where L marks a laser field and ST denotes the plasma electrostatic field. In the frame of the TWA the following equations are obvious:

$$E_{ST,Y} = 0, \quad \frac{\partial j_Y}{\partial y} = 0, \quad \frac{\partial A_L}{\partial y} \approx \cos \theta \frac{\partial A_L}{\partial t},$$

where $A_L = H_z, \mathbf{E}_L$. Then, by excluding $E_{L,X}$ and by introducing $H_0 = \sin \theta H_z$, Eq. (5) can be reduced to the one-dimensional form,

$$\begin{aligned} -\frac{\partial H_0}{\partial x} &= \sin \theta \frac{\partial E_{L,Y}}{\partial t} + j_Y \sin \theta, & \frac{\partial E_{L,Y}}{\partial x} - \left(j_X + \frac{\partial E_{ST,X}}{\partial t} \right) \cos \theta &= -\sin \theta \frac{\partial H_0}{\partial t}, \\ E_{L,X} &= H_z \cos \theta + \int_0^t dt' \left(j_X + \frac{\partial E_{ST,X}}{\partial t'} \right), & \frac{\partial E_{L,X}}{\partial x} &= \frac{\partial H_z}{\partial x} \cos \theta, & \frac{\partial E_{ST,X}}{\partial x} &= \rho. \end{aligned} \quad (6a)$$

Equation (6a) can also be rewritten in the form of two plane waves,

$$\begin{aligned} \frac{\partial}{\partial x} A_{\pm} \pm \sin \theta \frac{\partial}{\partial t} A_{\pm} &= -\frac{1}{2} j_Y \sin \theta \mp \frac{1}{2} \cos \theta \left(j_X + \frac{\partial E_{ST,X}}{\partial t} \right), \\ H_z &= (A_+ + A_-) / \sin \theta, & E_{L,Y} &= A_+ - A_-, \\ E_X &= E_{L,X} + E_{ST,X}, & E_{L,X} &= (A_+ + A_-) \cos \theta / \sin \theta, \\ \frac{\partial(1 + \chi) E_{ST,X}}{\partial x} &= \rho, \end{aligned} \quad (6b)$$

where A_+ and A_- are the fields of incoming and outgoing waves moving with the velocity $\sin \theta^{-1}$ and $\sin \theta^{-1}$, respectively, in the x direction, with χ as the implicit susceptibility [17,23]. The absorption efficiency η is determined by the following equation:

$$\eta = 1 - \int dt A_-^2(t, x) / \int dt A_+^2(t, x).$$

Equation (6) exactly corresponds to the one-dimensional approximation [9] which used a relativistic frame of reference moving with $u_y = -\cos \theta$. This can be shown by substituting

the fields, current components, and charge density determined in the laboratory reference frame to the Maxwellian equations in the relativistic reference frame,

$$\begin{aligned} E_X^{r1} &= (E_X^{\text{lb}} - H_Z^{\text{lb}} \cos \theta) / \sin \theta, \\ H_Z^{r1} &= (H_Z^{\text{lb}} - E_X^{\text{lb}} \cos \theta) / \sin \theta, & E_Y^{r1} &= E_Y^{\text{lb}}, \\ j_Y^{r1} &= (j_Y^{\text{lb}} + \rho \cos \theta) / \sin \theta, & j_X^{r1} &= j_X^{\text{lb}}, \\ \rho^{r1} &= (\rho^{\text{lb}} + j_Y^{\text{lb}} \cos \theta) / \sin \theta, \end{aligned}$$

where the lb marks the values in the laboratory frame and the rl in the relativistic frame. But the laboratory reference frame is much preferable for nonrelativistic plasmas by letting us avoid the noise due to appearance of the plasma charge density in the Maxwellian curl equations. Equation (6b) is the well-known normally incident-wave equation [15] at $\theta = \pi/2$.

The boundary conditions for Eq. (5) are trivial. The incoming field is equal to the laser at the right side of the plasma, and the outgoing field is zero at the left side.

C. Average ion approximation

Even during a short laser pulse there is essential collisional ionization of plasma because of high plasma density [13,15]. For example, by using the Lotz formula for the collisional ionization cross section,

$$\sigma_Z \approx 4 \times 10^{-14} \xi \frac{\ln(\epsilon/I_Z)}{\epsilon I_Z} \text{cm}^2, \quad (7)$$

where I_Z is the ionization energy in eV, ξ is the number of equivalent electrons in an ion shell, ϵ is the electron energy in eV, and assuming that the plasma density N_0 is equal to $5 \times 10^{22} \text{cm}^{-3}$ and electron energies are about 100 eV, we get the ionization time τ_i equal to $\tau_i(I_Z=100 \text{eV})=5 \text{fs}$. This time is much shorter than the pulse duration, but already for $I_Z=500 \text{eV}$, $\tau_i > 100 \text{fs}$ and can be longer than the laser pulse.

In the PIC simulation any ionization process can be included by allowing the change of superparticle charges. First, we introduce the ‘‘kinetics’’ grid along with the grid for the PIC. Many PIC cells (>20) are enclosed into a ‘‘kinetics’’ cell to provide good statistics for the electron density, temperature, and average ion charge. For an ideal plasma the sense of the ‘‘kinetics’’ cell is obvious. The density and temperature can be really determined within the length that includes, at least, several free paths of plasma electrons and much exceeds the length of the PIC cell which approximately equals the Debye radius. The ‘‘kinetics’’ grid simply represents the scale for macroscopic plasma parameters, as the PIC grid presents the electromagnetic field scale. Any process with a typical length that is less than the Debye radius or the size of the PIC cell has to be included in the Langevin equation. If the PIC cell excessively exceeds the Debye radius the Langevin equation has to be modified to the LB equation (1) to describe the particle scattering by plasma short wave fields.

The change in the electron charge in every ‘‘kinetics’’ cell is calculated by the standard balance equations for plasma electrons in the frame of the average ion approximation,

$$\frac{dQ_{ek}}{dt} = N_Z \left[-Q_{ek}(R_Z N_e) + \sum_{\epsilon_l > I_Z} q_l v_l \sigma_Z(v_l) + \frac{\alpha}{\tau(I_{Z+1}, E_k)} \right], \quad (8a)$$

where Q_{ek} is the total electron charge in the k th ‘‘kinetics’’ cell, q_l is the charge of the l th electron superparticle, the ionization cross section σ_Z is used in the form (7).

$$R_Z = CZ^3/T_e^{9/2}, \quad C = 6 \times 10^{-27} \text{cm}^6 \text{eV}^{9/2}/\text{s}$$

is the three-body recombination rate. Field ionization, including optical field ionization (OFI) is included by introducing the optical field ionization probability, $\tau^{-1}(I_Z, E_k)$ [24], where E_k is the effective electric field in the k th ‘‘kinetics’’ cell. In Eq. (8) α is a normalization constant. The effective current approximation [25] is used to include the energy loss. Excited states are not presented in the model. The ionization energy I_Z is continuously changed with average ion charge, Z , and is fitted to be equal to a realistic energy at an integer Z . The charge change by Eq. (8a) is determined after every time step and redistributed over all ion and electron superparticles belonging to a ‘‘kinetics’’ cell. The charges of the superparticles are changed by adding

$$\Delta q_{ek} = \Delta Q_{ek}/N_{ke}, \quad \Delta q_{ik} = -\Delta Q_{ek}/N_{ki}, \quad (8b)$$

where N_{ke} and N_{ki} are the number of the electron and ion superparticles, respectively, in the cell. The energy of the particle producing the new charge is decreased on

$$\Delta \epsilon_l = N_0 v_l \sigma_Z(v_l) I_Z \Delta t.$$

The plasma parameters like the electron temperature, density, and average ion charge in a ‘‘kinetics’’ cell are recalculated after every time step.

Two species of charge are attached for every ion superparticle. The first one, Q_{ik} , is the charge of an ion superparticle which is changed according to Eq. (8). The second, Q_{ik}^0 , is a constant which is equivalent to a unit ion charge and is used for calculation of the ion charge to be included in the motion equation (2). The electron density is obtained by weighting the superparticle charge density in the ‘‘kinetics’’ cell. A similar procedure with Q_{ik}^0 is used to get the ion density. The temperature and the mean velocity of the plasma electrons are determined by simple averaging that uses the charge of the superparticle as its weight.

D. Particle-in-cell portion

To solve Eqs. (2), (3), and (6) the 1D3V relativistic electromagnetic code [17] with square current and charge weighting is used. Both the direct-implicit (C1) scheme [26] and the leapfrog scheme [18] are employed. We could not completely use the advantage of the direct-implicit scheme because of the high laser frequency. Collisions are computed as an effective force after calculation of the velocity and position of particles. The kinetic parameters such as the temperature and densities are determined on the ‘‘kinetics’’ grid for every calculation step.

The boundary conditions for superparticles in the system under consideration are not trivial. In the present calculation a superparticle accelerated over the system boundary in the laser side is kept at the boundary. The charge of such a superparticle is involved in the electrostatic field calculation. The velocity of a superparticle accelerated over the system boundary in the plasma side is redistributed within the Maxwellian velocity distribution with the plasma temperature.

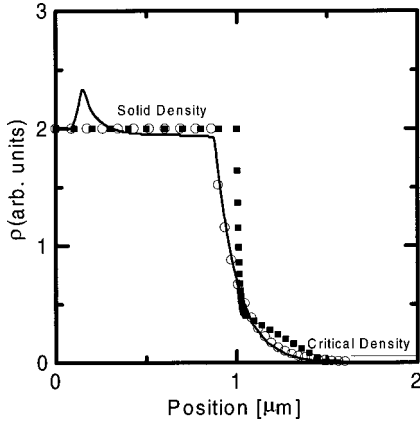


FIG. 1. Plasma density profiles. The curve represents a typical density distribution obtained from a hydrodynamic simulation of the steep-like density plasma expansion. The open circles and filled squares represent profiles used for PIC simulation.

III. RESULTS OF SIMULATION

The present calculations are carried out for silicon and carbon plasmas of solid-density $N_{\text{solid}} = 5 \times 10^{22} \text{ cm}^{-3}$. The plasma size is varied from 0.25 to 1 μm depending on the laser intensity and angle of incidence. The two plasma density profiles at the right (laser) side of plasma, $x > 0$, are chosen for the simulation. The first is a linear profile,

$$N(x) = N_1 \left(1 - \frac{N_{\text{cr}} x}{N_1 L} \right), \quad N_{\text{cr}} < N_1 < N_{\text{solid}} \quad (9a)$$

and the second is an exponential profile,

$$N(x) = N_{\text{solid}} e^{-x/L}, \quad (9b)$$

where L is the density gradient in the vicinity of the critical density. $N(x < 0) = N_{\text{solid}}$. The presentation (9) for the plasma density is a good approximation for density profile formed after plasma expansion due to laser prepulse (see, Fig. 1). The value of L determined by the prepulse delay is varied from 0.0 to 0.6 μm . The initial electron temperature is chosen equal to 10 and 20 eV for silicon and carbon plasmas, respectively. The initial velocity distribution of plasma electrons is the Maxwellian. The fluid velocity linearly increasing toward the plasma surface is suggested. Initially the ion charge is uniform over the plasma, and the ion and electron densities are equal. The wavelength and intensity of laser, pulse duration, incident angle, and also L are parameters.

To provide stability the number of superparticles used is around 70 000 per 1 μm of plasma. The number of PIC cells is varied from 8000 to 16 000 and that of ‘kinetics’ cells from 200 to 600. The time step grows from the initial value of 0.1 to 0.36 of the plasma oscillation period due to the ionization. The plasma bulk in the simulations is divided into two parts, in accordance with Eq. (9), and two different species of superparticles are used for the simulation. The charges of the superparticles which represent electrons and ions for each kinetics cell are changed following the rule described in the preceding section. The intensity of the laser pulse is constant.

A. Heat flow and ionization dynamics in plasmas irradiated by normally incident pulse

The heat flow and the ionization dynamics in a plasma with elastic collisions irradiated by a normally incident subpicosecond laser pulse is a good check for the method due to its ability to quantitatively compare the results of the PIC and Langevin simulation with those in [15] obtained by direct solution of the FP equation.

In the following [15] we consider a solid-density carbon plasma irradiated by a normally incident pulse of a KrF laser ($\lambda = 248 \text{ nm}$). The initial temperature of the plasma is chosen to be 20 eV and initial ion average charge is set to $Z = 1.5$. In contrast to [15], instead of assuming the amount of energy deposited on the plasma surface, the laser intensity for the deposited energy is chosen to be equal to that used for FP calculation ($750 \text{ TW/cm}^2 \times 300 \text{ fs}$). We chose $I = 10^{16} \text{ W/cm}^2$. The steep density gradient at the plasma surface, $L = 0$, is considered. Both electron-electron and electron-ion collisions are involved in the simulation in the frame of the Langevin equation (2), (3).

The evolution of the absorption efficiency is determined by the transient ionization and plasma heating. In this case, the absorption is dominated by collisions, and the efficiency can be estimated by using the following equation [6]:

$$\eta \approx \begin{cases} \frac{2\gamma_{ei}}{\omega_{\text{pl}}} \sim \left(\frac{Z}{T_e} \right)^{3/2}, & \gamma_{ei} < \omega \\ \frac{2\omega}{\omega_{\text{pl}}} \left(\frac{\gamma_{ei}}{\omega_{\text{pl}}} \right)^{1/2} \sim \left(\frac{Z}{T_e^3} \right)^{1/4}, & \gamma_{ei} > \omega \end{cases} \quad (10)$$

where γ_{ei} is the collision frequency and Z is the ion charge. Because the ion charge is increased from 1.5 to 5, and T_e rises by more than ten times, the absorption efficiency slightly decreases during the laser pulse from 10% to 8%. Finally, the absorbed energy is very close to that used in [15]. At the beginning of the heating process the ionization takes a large portion of the absorbed laser energy. After the average ion charge exceeds 4 (Li-like carbon) the energy of the plasma electron is not enough for efficient ionization of He- and H-like ions. Then the deposited laser energy is mainly utilized by plasma electrons through heat transfer. Initially the heating occurs only in the skin layer determined by electron-ion collisions. The energy of the quiver in this case is not high, it is approximately 50 eV, and a certain amount of time is needed for plasma heating. As the average ion charge in the skin layer is increased due to the electron collisional ionization the heating in the skin layer also increases so that the collisional time is almost constant.

Good agreement between the results of the present calculation of the temperature and electron density distribution inside the plasma after laser pulse and those in Ref. [15] are shown in Figs. 2(a) and 2(b). Because the heat flow and ionization, due to heating, are dominated by collisions, the result proves the correctness of using the Langevin equation. The discrepancy of the results on the plasma surface is due to the effect of fast electrons and ion motion which have not been included in the FP calculation [15]. Also, good agreement of the PIC and Langevin equation simulation for a steep temperature gradient decay with that of FP can be found in [27].

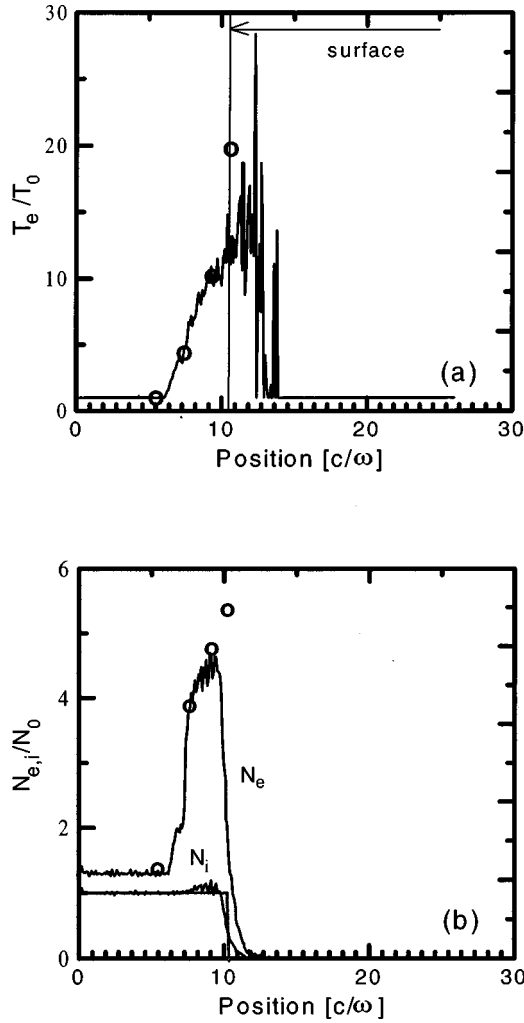


FIG. 2. Spatial distribution of the electron temperature (a) and density (b) in a solid C plasma irradiated by a normally incident pulse of a KrF laser with the intensity of $I=10^{16}$ W/cm 2 at $t=0.3$ ps. The initial temperature is $T_0=20$ eV. The circles represent the electron temperature and ion charge distribution from the direct Fokker-Plank simulation [15].

We should point out that electron-electron collisions do not notably affect the absorption efficiency and ionization balance because of the high average ion charge ($Z>4$) in the heated skin layer, but they do until the effect of the fast electrons becomes negligible.

B. Absorption of p -polarized obliquely incident pulse laser

Self-consistent simulation of the absorption of a p -polarized, obliquely incident pulse laser by solid-density plasmas along with ionization dynamics has not been carried out, although it is obvious that the ionization process may affect not only the heat flow but also the plasma reflectivity. In the present work, the hybrid particle-in-cell method with the TWA is applied to model the absorption of a p -polarized pulse laser with the parameters of the experiment [17], the wavelength $\lambda=800$ nm and intensity $I=4\times 10^{16}$ W/cm 2 by a silicon plasma. The calculations are carried out for various density gradients and incident angles.

The temporal evolution of the electric and magnetic fields in the presence of a p -polarized laser pulse is not trivial (see,

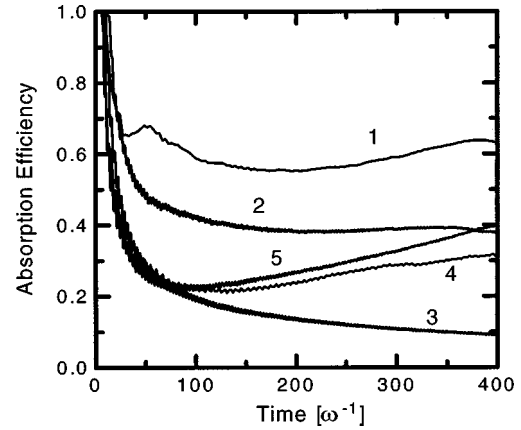


FIG. 3. Absorption efficiency of a Si plasma irradiated by a $\lambda=800$ -nm, (1)–(4) $I=4\times 10^{16}$ W/cm 2 and (5) $I=4\times 10^{17}$ W/cm 2 , p -polarized pulse laser [17] with the prepulse $T_0=10$ eV, $N_1=1.2\times 10^{22}$ cm $^{-3}$. (1)–(2) $L=0.22$ μ m; (3)–(5) $L=0$ at incident angles, $\pi/2-\theta$: (1), (4), (5) 45°; (2) 20°; (3) 0°.

for example, [9,12]) and is dominated by vacuum heating and resonance absorption. Due to resonance absorption the x component of the electric field is compressed in the vicinity of the critical density and accelerates a part of the plasma electrons outward. The locking electrostatic field then grows and low energy electrons cannot leave the plasma. With the increase of the ion charge Z the plasma conductivity decreases due to electron-ion collisions and the electrostatic field in the plasma increases to prevent the charge separation that leads to increase in the energy of fast electrons. Even for a steep density gradient, $L=0$, plasma electrons are accelerated by the x component of the laser electric field which produces the electrostatic field near the plasma surface.

The absorption efficiency due to anomalous skin effect, vacuum heating, and collisions can be estimated for the steep density gradient plasma (see [6] and references there). So, efficiency due to the anomalous skin effect is

$$\eta \approx \left(\frac{v_{Te} \omega^2}{c \omega_{pl}^2} \right)^{1/3},$$

and, for the parameters of [17], is about 10%. The efficiency of the vacuum heating,

$$\eta \approx 3 \frac{\cos^3 \theta}{\sin \theta} \frac{v_{os}}{c},$$

where v_{os} is the quiver velocity, is small, about a few percent for $\theta \geq \pi/4$. The efficiency of the collisional absorption, Eq. (10), is about 10%. This means the total efficiency due to these processes is hardly higher than 20%. The result of the simulation of the normally and obliquely incident p -polarized pulse absorption by a plasma with very steep density gradient without ion motion is in good agreement with the estimations.

Some of the results obtained are presented in Figs. 3 and 4. The temporal evolution of the absorption efficiency for a plasma with different density gradient in the vicinity of the critical point, and different laser polarization and intensity is shown in Fig. 3. For a plasma with density gradient, which is formed by the laser prepulse, that is optimal for the reso-

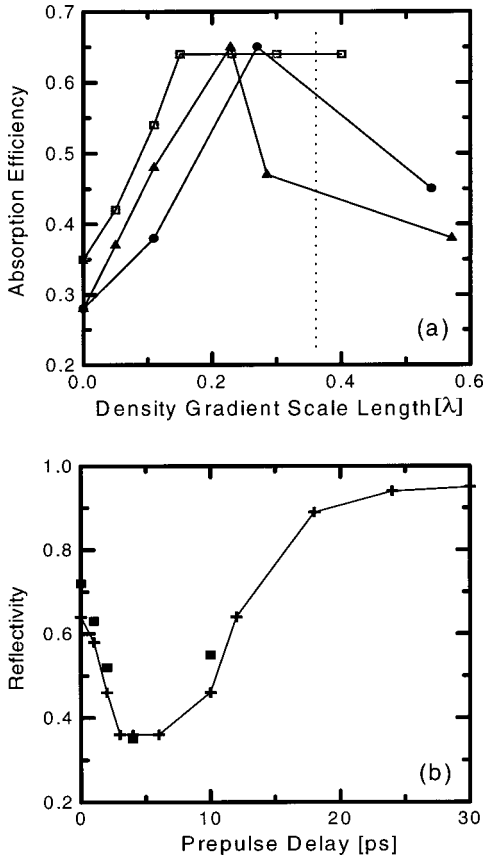


FIG. 4. Absorption efficiency versus the initial density gradient in the vicinity of the critical point (a). Filled circles, the linear profile; triangles, the exponential profile; squares, the results of [17]. The vertical line is the maximal density gradient measured in [17]. Efficiency versus the prepulse delay τ (b). The squares represent the reflectivity of the p -polarized pulse (45°), the crosses are the results of [17].

nance absorption (curve 1), the absorption efficiency is high, about 70%, and is almost constant during the laser pulse. This means that the ion motion, during laser pulse, does not affect the efficiency of the resonance absorption. Due to the resonance character of the absorption, its efficiency decreases with the laser incidence angle (curve 2). In the case of the steep density gradient $L=0$, the temporal evolution of absorption efficiency (curves 3, 4) is dependent on the plasma ionization. For the intensity under consideration, the collisional ionization of the plasma is dominant and, because of high density of the plasma, produces multiple charged ions during the laser pulse. Heavy plasma ions are accelerated by the electrostatic field, because of the high ratio of $Z/M_i < 1/3m_H$ (m_H is the hydrogen mass) that results in the resonance absorption process. The absorption efficiency of the plasma increases with the laser intensity both due to faster ionization and due to higher electrostatic field near the plasma surface. The effects of the OFI and ionization by the compressed electrostatic field are much less efficient than the collisional ionization for intensity which is less than 10^{18} W/cm². We have to note that according to our calculation the time of optimal absorption is as much as two times longer than the time given in [12] due to transient plasma ionization. Curve 5 in Fig. 3 shows the temporal evolution of the absorption efficiency for the normally incident pulse. Be-

cause the collisions dominate the absorption process for moderate laser intensity, the efficiency is small, less than 10%, and is in accordance with Eq. (10).

We obtained the maximum absorption efficiency ($\eta = 67\%$) at $N_1 = 1.2 \times 10^{22}$ cm⁻³, $L = 0.22$ μ m, and incident angle of 45° . If initially the plasma boundary being heated by a laser prepulse has the velocity $(1-2) \times 10^7$ cm/s, it passes the distance $S = N_1 L / N_{Cr}$ in the time $\tau = 4-8$ ps. Hydrodynamics calculation for a solid-density Si plasma with a steep temperature distribution gives the same time delay for the optimal density gradient. Figures 4(a) and 4(b) represent the dependence of the measured [17] and computed reflectivity of a silicon plasma on the density gradient in the vicinity of the critical point (a) and the prepulse delay (b). The latter was plotted by using the measured dependence of the density gradient on the prepulse delay [17] which coincides with one from hydrodynamics calculation. The numerical results are in a good agreement with the experimental ones when the resonance absorption occurs. For the very steep density gradient the numerical absorption efficiency (30%) is less than the one measured (35%) in [17].

C. Heat flow in plasmas irradiated by p -polarized pulse

The heat in the case of an intense, obliquely incident p -polarized pulse laser is carried inward by fast electrons produced by collisionless absorption processes. In this case, the return current plays an important role in the heat transfer [16]. To estimate the penetration of fast electrons we assume that all deposited power, $W = \eta I$, is taken by fast electrons with energy $\langle \varepsilon \rangle$,

$$W = \eta I = \langle \varepsilon \rangle j_{\text{fast}} / e, \quad (11a)$$

where η is the efficiency, I is the laser pulse intensity, and j_{fast} is the density of the fast electron current. To provide the plasma neutrality the fast electron current must be compensated by the return current, j_{pl}

$$j_{\text{fast}} = j_{\text{pl}} = \sigma E \approx \frac{e^2 N_e^{\text{solid}}}{m_e \gamma_{ei}}, \quad (11b)$$

where E is the electric field in the plasma, σ is the plasma conductivity, and γ_{ei} is the electron-ion collision frequency. According to Eq. (11b) the density of the deposition energy can be found by the equation

$$\frac{dW}{dx} = -j_{\text{pl}} E = -W^2 \frac{m_e \gamma_{ei}}{N_e^{\text{solid}} \langle \varepsilon \rangle^2}, \quad W(0) = \eta I. \quad (12)$$

The deposition depth can be easily estimated by solving Eq. (12),

$$l_D = \frac{N_e^{\text{solid}} \langle \varepsilon \rangle^2}{\eta I (m_e \gamma_{ei})} = \frac{m_e v_{T_e}^3 \langle \varepsilon \rangle^2}{4 \pi \Lambda \eta I e^4 \langle Z \rangle}.$$

For $T_e = 100$ eV, $\langle Z \rangle = 1$, $\langle \varepsilon \rangle = 3$ keV, $I = 4 \times 10^{16}$ W/cm², and $\eta = 0.3$ the depth is 0.1 μ m. Because the ratio $\langle \varepsilon \rangle^2 / I$ weakly depends on the intensity the value of the depth is mainly determined by the temperature of a solid-density plasma. An increase in the average ion charge leads to a decrease of the deposition depth.

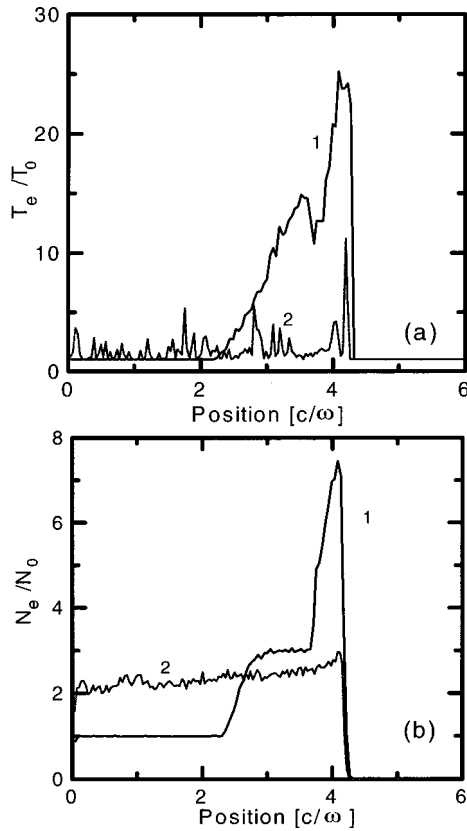


FIG. 5. Electron temperature (a) and density (b) distributions in the silicon plasma, $L=0$, irradiated by a $\lambda=800$ -nm, $I=4 \times 10^{16}$ W/cm², p -polarized pulse laser [17]. $T_0=10$ eV, $\omega t=200$. (1) collisional; (2) collisionless plasmas.

It is found that when the absorption due to vacuum heating or due to resonance absorption is dominant, the ionization balance and heat transfer into an overdense plasma, and, as a result, its x-ray emission can be determined by elastic collisions. The results are illustrated by Figs. 5(a) and 5(b) where the instantaneous electron temperature and density in collisional (1) and collisionless (2) plasmas are presented. The efficiency of the absorption by a collisionless plasma due to the anomalous skin effect and the vacuum heating is not small, about 10%, and is almost equal to the efficiency of the collisional absorption. But the electron temperature and density distributions in the collisionless plasma are totally different from those of a plasma with elastic collisions. It is the result of the very small resistivity of collisionless plasma. The beamlike fast electrons produced by vacuum heating can easily penetrate the plasma bulk. In contrast to that, the fast electrons in the collisional plasma, being decelerated by the internal electrostatic field which arises because of the plasma resistivity, deposit their energy near the plasma surface.

The role of the return current in plasma ionization is illustrated in Figs. 6(a) and 6(b). The electron temperature (a) and density (b) distributions are calculated for plasma parameters at which the resonance absorption is dominant. Hence, the absorbed energy is mainly utilized for electron acceleration. The return current then is determined by the electron runaway in the electrostatic field produced by the fast electrons. If only electron-ion collisions occur [curve 2 in Fig. 6(a)] the plasma conductivity is small and only high energy electrons can penetrate the plasma because of charge

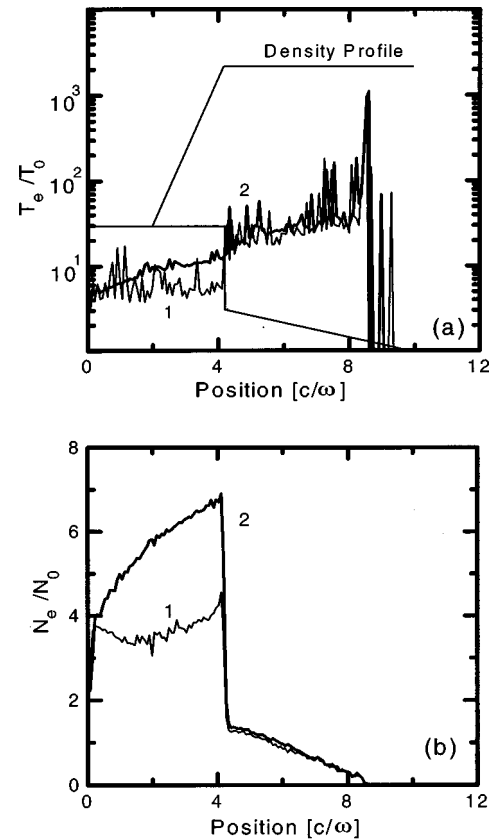


FIG. 6. Typical electron temperature (a) and density (b) distributions in a silicon plasma irradiated by a $\lambda=800$ -nm, $I=4 \times 10^{16}$ W/cm², p -polarized pulse laser [17] with density distribution determined by Eq. (8a) for $L/\lambda=0.22$ (4–6 ps prepulse delay). $T_0=10$ eV, $t=120$ fs. (1) $e-e$ and $e-i$ collisions are included; (2) only $e-i$ collisions are included.

separation. The ionization in the plasma bulk is dominated by those fast electrons. Only Si^{+4} and Si^{+5} ions are mainly presented in the plasma bulk [curve 2 in Fig. 6(b)]. With electron-electron collisions the runaway rate increases and the conductivity also increases [19], and the heat transfer speeds up. Because the energies of the runaway electrons are less than those of the fast electrons, the ionization by the electron from the return current is more efficient. The Si^{+7} ions appear near the plasma surface where the effect of the electrostatic field is the strongest.

Figures 7(a) and 7(b) show the temporal evolution of the electron temperature and density distribution in a Si plasma with a steep density gradient irradiated by a laser pulse of intensity $I=4 \times 10^{17}$ W/cm². There is not sufficient field ionization yet and the heat transfer and plasma ionization are steered by collisions. The plasma temperature does not exceed 1 keV during the laser pulse. Upon being heated up to 1 keV, the plasma acts collisionless. Because there is no further Ohmic heating by the return current the plasma temperature distribution is flattened, while the electron density is still nonuniform because of ionization delay.

IV. SUMMARY

The effect of variable ionization and elastic collisions is found to change the heat transfer process by fast electrons

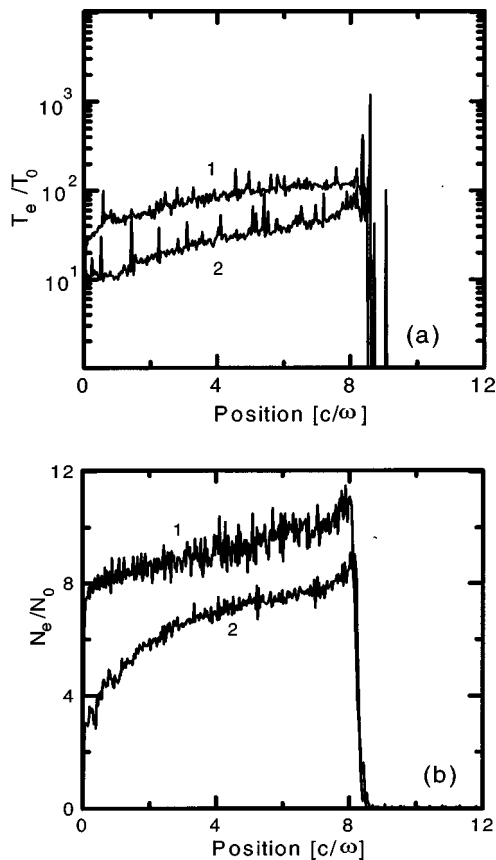


FIG. 7. Electron temperature (a) and density (b) distributions in a silicon plasma, $L=0$, irradiated by a $\lambda=800$ -nm, $I=4 \times 10^{17}$ W/cm², p -polarized (45°) pulse. $T_0=10$ eV; (1) $t=140$ fs; (2) $t=70$ fs.

into the overdense plasma irradiated by an obliquely incident p -polarized pulse laser by changing the plasma conductivity. Due to collisions, the penetration depth of fast electrons produced by the vacuum heating and resonance absorption is much smaller than that of collisionless plasmas. The Ohmic heating due to the return current is responsible for energy deposition. Having less energy than electrons accelerated by laser, electrons in the return current ionize plasma more efficiently. Electron-electron collisions dominate the energetic part of the distribution of return current electrons that results

in plasma ionization and, hence, in the heat transfer. By increasing ion charges on the irradiated surface, the transient ionization changes the absorption rate more rapidly. The absorption efficiency of a p -polarized pulse (wavelength $\lambda=800$ nm, duration $T=120$ fs, $\theta=45^\circ$) with intensity $I=4 \times 10^{16}$ – 4×10^{17} W/cm² for Si plasmas with a steep density gradient is increased from 20% to 30–40% due to ion acceleration.

To examine these processes three approaches are suggested: the one-dimensional particle-in-cell method in conjunction with the use of the Langevin equation for elastic electron collisions to conform to a direct solution of the Fokker-Plank-Landau equation; the two-wave approximation to allow the obliquely incident p -polarized laser-plasma interaction simulation in the laboratory reference frame; the method of redistribution of variable superparticle charges into the “kinetics” grid cells to include the atomic physics processes in PIC simulation. The method is used for simulation of the heat transfer in a carbon plasma, with elastic collisions and variable ionization, irradiated by a normally incident pulse of a KrF laser. The laser absorption is computed self-consistently. The spatial distribution of the electron density and temperature after $t=0.3$ ps of laser irradiation agrees well with those obtained by direct FPL simulation [15]. The calculation of the efficiency of the obliquely incident p -polarized laser absorption by a plasma with density profile determined by a prepulse shows that the absorption is mainly determined by vacuum heating and anomalous skin effect with a steep density gradient and then is dominated by the resonance absorption as the density scale length near the critical surface increases. The effect of prepulse delay is in forming a plasma corona. With the prepulse delay the density gradient near the critical surface passes the optimum for the resonance absorption. The results of calculation of the absorption efficiency are in good agreement with experiments [17].

ACKNOWLEDGMENTS

The authors would like to thank Professor T. Tajima, Dr. Y. Kishimoto, Dr. Y. Ueshima, and Dr. K. Moribayashi for useful discussions and Dr. H. Ihara and Dr. T. Arisawa for encouraging this research.

-
- [1] J. A. Cobble, G. T. Schappert, L. A. Jones, A. J. Taylor, G. A. Kyrala, and R. D. Fulton, *J. Appl. Phys.* **69**, 3369 (1991).
 - [2] A. Rouse, P. Audebert, J. P. Geindre, F. Fallies, J. C. Gauthier, A. Mysyrowicz, G. Grillon, and A. Antonetti, *Phys. Rev. E* **50**, 2200 (1994).
 - [3] T. Feurer, W. Theobald, R. Sauerbrey, I. Uschmann, D. Altenbernd, U. Teubner, P. Gibbon, E. Forster, G. Malka, and J. L. Miquel, *Phys. Rev. E* **56**, 4608 (1997).
 - [4] S. E. Harris and J. D. Kmetec, *Phys. Rev. Lett.* **61**, 62 (1988).
 - [5] R. Kauffman, in *Handbook of Plasma Physics*, edited by M. N. Rosenblut and R. Z. Sagdeev, *Physics of Laser Plasma Vol. 3*, edited by A. M. Rubenchik and S. Witkovski (North-Holland, Amsterdam, 1991), p. 111.
 - [6] P. Gibbon and E. Forster, *Plasma Phys. Controlled Fusion* **38**, 769 (1996).
 - [7] F. Brunel, *Phys. Rev. Lett.* **59**, 52 (1987).
 - [8] W. Rozmus and V. T. Tihonchuk, *Phys. Rev. A* **42**, 7401 (1990).
 - [9] P. Gibbon and A. R. Bell, *Phys. Rev. Lett.* **68**, 1535 (1992).
 - [10] S. C. Wilks, W. L. Kruer, M. Tabak, and A. B. Langdon, *Phys. Rev. Lett.* **69**, 1383 (1992).
 - [11] J. Denavit, *Phys. Rev. Lett.* **69**, 3052 (1992).
 - [12] P. Gibbon, *Phys. Rev. Lett.* **73**, 664 (1994).
 - [13] J. P. Matte, J. C. Keiffer, S. Ethier, M. Chaker, and O. Peyrusse, *Phys. Rev. Lett.* **72**, 1208 (1994).
 - [14] T.-Y. B. Yang, W. L. Kruer, R. M. More, and A. B. Langdon, *Phys. Plasmas* **2**, 3145 (1995).
 - [15] R. P. Town, A. R. Bell, and S. J. Rose, *Phys. Rev. Lett.* **74**, 924 (1995).

- [16] A. R. Bell, J. R. Davies, S. Guerin, and H. Ruhl, *Plasma Phys. Controlled Fusion* **39**, 653 (1997).
- [17] S. Bastiani, A. Rousse, J. P. Geindre, P. Audebert, C. Quiox, G. Hamoniaux, A. Antonetti, and J. C. Gauthier, *Phys. Rev. E* **56**, 7179 (1997).
- [18] C. K. Birdsall and A. B. Langdon, *Plasma Physics, via Computer Simulation* (McGraw-Hill, New York, 1985).
- [19] A. G. Zhidkov, *Phys. Plasmas* **5**, 385 (1998).
- [20] R. Balescu, *Phys. Fluids* **3**, 52 (1960).
- [21] A. Lenard, *Ann. Phys. (N.Y.)* **3**, 90 (1960).
- [22] B. A. Trubnikov, in *Reviews in Plasma Physics*, edited by M. A. Leontovich (Consultants Bureau, New York, 1965), Vol. 1, p. 95.
- [23] R. M. More, in *Handbook of Plasma Physics*, edited by M. N. Rothenbluth and R. Z. Sagdeev, *Physics of Laser Plasma Vol. 3*, edited by A. M. Rubenchik and S. Witkovsky (North-Holland, Amsterdam, 1991), p. 63.
- [24] M. V. Amosov, N. B. Delone, and V. P. Krainov, *Zh. Eksp. Teor. Fiz.* **91**, 2008 (1986) [*Sov. Phys. JETP* **64**, 1191 (1986)].
- [25] S. C. Rae and K. Burnett, *Phys. Rev. A* **46**, 1084 (1992).
- [26] B. I. Cohen, A. B. Langdon, and D. W. Hewett, *J. Comput. Phys.* **81**, 151 (1989).
- [27] A. Zhidkov and A. Sasaki, JAERI-Research Report No. 98-068, 1998.